Calculation of strong-field magnetoresistance in some periodic composites

David J. Bergman
School of Physics and Astronomy, Raymond and Beverly Sackler Faculty of Exact Sciences, Tel Aviv University, Tel Aviv 69978, Israel

Yakov M. Strelniker
School of Physics and Astronomy, Raymond and Beverly Sackler Faculty of Exact Sciences, Tel Aviv University, Tel Aviv 69978, Israel
and Jordan Valley College, Jordan Valley 15132, Israel

(Received 7 December 1993)

A calculational method based on Fourier expansion is applied to a study of the strong-field magnetotransport of a uniform free-electron metal, inside which is embedded a simple cubic array of identical spheres or cylinders, which have a different conductivity tensor. When the magnetic field is strong enough, the magnetoresistance exhibits very strong variations with the direction of the field. This can be understood in some of the cases by simple physical considerations about the distortions induced in the current flow by the inclusions. The strong dependence on the field direction is qualitatively, and sometimes even quantitatively, similar to what is observed in some metallic crystals which have a noncompact Fermi surface.

I. INTRODUCTION

Measurements of magnetotransport in composite conductors are quite rare, especially in comparison with the widespread use of Hall and magnetoresistance measurements in the study and characterization of uniform conductors. Those few experimental studies that have been reported are confined to the domain of disordered composite media.[1,2] Not surprisingly, perhaps, theoretical discussions have also been confined, until now, to disordered composites, especially near a percolation threshold,[3–18] where interesting behavior was predicted and, in some cases, observed.[1] In these works the results were always independent of the direction of the magnetic field $\mathbf{H}$, as a consequence of the statistical isotropy of the disordered composite medium. However, in a composite medium with periodic microstructure, it is reasonable to expect that some of these properties will be anisotropic. Even for the case of a cubic lattice, for which the resistivity tensor is a scalar when $\mathbf{H} = \mathbf{0}$, the presence of a nonzero $\mathbf{H}$ can lead to a strong anisotropy of the magnetoresistance. This is well known from the study of metallic crystals,[19,20] but has never been studied in the context of a composite conducting medium.

We report here on some results of a theoretical and numerical study of strong-field magnetotransport in a composite conductor with a periodic microstructure, namely, a simple cubic array of spheres or cylinders embedded in an isotropic conducting host medium which is taken to be a free-electron metal without any intrinsic magnetoresistance. The inclusions are either insulating, or else conductors that are also of the free-electron-metal type, but with a different value of the Hall conductivity than that of the host medium. When the magnetic field $\mathbf{H}$ is strong enough, we find a strong dependence of the bulk effective Ohmic resistivities upon $\mathbf{H}$. Moreover, both the transverse and the longitudinal resistivities exhibit a strong dependence on the direction of $\mathbf{H}$, including a sequence of maxima and minima, the appearance of which can be understood, in some of the cases, from a simple physical argument.

The remainder of this paper is organized as follows: In Sec. II we summarize the technique used to evaluate the effective conductivity tensor (a more detailed description will be published elsewhere[21]) and discuss the procedure of calculating the transverse and longitudinal components of the resistivity tensor. In Sec. III we present numerical results for a composite with spherical inclusions and in Sec. IV we do likewise for the case of cylindrical inclusions. Section V provides a discussion and summary of those results.

II. A SHORT DESCRIPTION OF THE CALCULATIONAL METHOD

We consider a two-component periodic composite made of two uniform conducting components, characterized by conductivity tensors $\hat{\sigma}_i$, $i = 1, 2$, which in the presence of a magnetic field have symmetric as well as antisymmetric parts. The position-dependent conductivity tensor $\hat{\sigma}(\mathbf{r})$ can be represented with the help of the characteristic or indicator function $\theta_1(\mathbf{r})$ of the $\hat{\sigma}_1$ component and the conductivity tensor difference $\delta\hat{\sigma}$, namely

$$\theta_1(\mathbf{r}) = \begin{cases} 1 & \text{for } \mathbf{r} \text{ inside } \hat{\sigma}_1 \\ 0 & \text{otherwise} , \end{cases} \tag{1}$$

$$\delta\hat{\sigma} \equiv \hat{\sigma}_2 - \hat{\sigma}_1 , \tag{2}$$

$$\hat{\sigma}(\mathbf{r}) = \hat{\sigma}_2 - \delta\hat{\sigma}\theta_1(\mathbf{r}). \tag{3}$$

The function $\theta_1(\mathbf{r})$ includes all the information about the system microstructure. Its volume average is just the volume fraction p_1 of the $\hat{\sigma}_1$ component.

The bulk effective conductivity tensor $\hat{\sigma}_e$ of the composite medium is defined by the relationship between the volume averages of the electric field $\nabla\phi$ and the current density $\mathbf{J} \equiv \hat{\sigma}\nabla\phi$

$$\langle \mathbf{J} \rangle \equiv \hat{\sigma}_e \langle \nabla\phi \rangle. \tag{4}$$

The local potential field $\phi^{(\alpha)}(\mathbf{r})$ which results when $\langle \nabla\phi \rangle = \nabla r_\alpha = \mathbf{e}_\alpha$, i.e., a unit vector in the α direction, is the solution of an integro-differential equation

$$\phi^{(\alpha)} = r_\alpha + \hat{\Gamma}\phi^{(\alpha)}, \tag{5}$$

$$\hat{\Gamma}\phi = \int dV' \theta_1(\mathbf{r}') \nabla' G(\mathbf{r}, \mathbf{r}' | \hat{\sigma}_2) \cdot \delta\hat{\sigma} \cdot \nabla' \phi(\mathbf{r}'), \tag{6}$$

where G is the Green's function for the $\hat{\sigma}_2$ component which vanishes at a pair of parallel equipotential planes. It can be found by solving the following boundary value problem:

$$\begin{gathered} \nabla \cdot \hat{\sigma}_2 \cdot \nabla G(\mathbf{r}, \mathbf{r}' | \hat{\sigma}_2) = -\delta^3(\mathbf{r} - \mathbf{r}') \ , \\ G = 0 \quad \text{when} \quad r_\alpha = 0, L. \end{gathered} \tag{7}$$

Clearly, the characteristic function $\theta_1(\mathbf{r})$ includes all the information about the microstructure or microgeometry of the medium. Because there is an asymmetry in this description, we will always take the $\hat{\sigma}_1$ component to represent the inclusions, while $\hat{\sigma}_2$ will represent the host medium.

The periodicity of the medium is exploited in order to expand ϕ in an appropriate Fourier series. This is possible whenever the finite thickness of the system L is large compared to the size of the unit cell. In that case, the results for $\hat{\sigma}_e$ will be independent of the thickness L. When L is not large enough, there will be size effects and surface effects—those will be discussed elsewhere. In the limit $L \to \infty$, the operator $\hat{\Gamma}$ can be represented by the infinite matrix

$$\Gamma_{\mathbf{g}\mathbf{g}'} = \frac{(\mathbf{g} \cdot \delta\hat{\sigma} \cdot \mathbf{g}')\theta_{\mathbf{g}-\mathbf{g}'}}{(\mathbf{g} \cdot \hat{\sigma}_2 \cdot \mathbf{g})^{1/2}(\mathbf{g}' \cdot \hat{\sigma}_2 \cdot \mathbf{g}')^{1/2}}, \tag{8}$$

where $\mathbf{g}, \mathbf{g}'$ are vectors of the reciprocal lattice and $\theta_{\mathbf{g}}$ is a Fourier coefficient of $\theta_1(\mathbf{r})$. Using this representation, the following series expansion in powers of $\delta\hat{\sigma}$ can be written for the elements of the matrix $\hat{\sigma}_e$ (note that a summation over the repeated tensor indices γ, ω is implied):

$$(\hat{\sigma}_2 - p_1\delta\hat{\sigma} - \hat{\sigma}_e)_{\alpha\beta} = \sum_{r=1}^{\infty} \delta\sigma_{\alpha\gamma} A^{(r-1)}_{\gamma\omega} \delta\sigma_{\omega\beta}, \tag{9}$$

$$A^{(r)}_{\gamma\omega} = \sum_{\mathbf{g}\neq 0} \sum_{\mathbf{g}'\neq 0} \frac{g_\gamma \theta_{-\mathbf{g}}}{(\mathbf{g} \cdot \hat{\sigma}_2 \cdot \mathbf{g})^{1/2}} (\hat{\Gamma}^r)_{\mathbf{g}\mathbf{g}'} \frac{g'_\omega \theta_{\mathbf{g}'}}{(\mathbf{g}' \cdot \hat{\sigma}_2 \cdot \mathbf{g}')^{1/2}}. \tag{10}$$

One way to obtain this result is first to solve (5) by iterating the integro-differential operator $\hat{\Gamma}$. The infinite series obtained in this way for ϕ is then used to calculate $\langle \mathbf{J} \rangle$ in (4), thus leading to the series for $\hat{\sigma}_e$. In order to calculate the coefficients $A^{(r)}_{\gamma\omega}$, we usually used truncated matrices $\Gamma_{\mathbf{g}\mathbf{g}'}$ which included $\mathbf{g}$ vectors, appropriate to a simple-cubic lattice, of the form $\mathbf{g} = \frac{2\pi}{b}(n_x, n_y, n_z)$, where b is the lattice constant and n_x, n_y, n_z are integers ranging as far as -10 to $+10$ in each direction, although sometimes, when the numerical calculation was very time consuming, we only included components of $\mathbf{g}$ ranging from -7 to $+7$ in each direction.

Instead of expanding in powers of $\hat{\Gamma}$, we could use the resolvent operator $1/(1-\hat{\Gamma})$ in order to calculate $\hat{\sigma}_e$. That would involve inverting the nonsparse matrix $1 - \hat{\Gamma}$, and would thus pose a severe limitation on the number of $\mathbf{g}$ vectors that can be included: if the components of $\mathbf{g}$ range from -5 to $+5$ in all directions, the size of the matrix $\Gamma_{\mathbf{g}\mathbf{g}'}$ is already 1330×1330, which is the largest that we are conveniently able to invert with existing workstations. The $\hat{\Gamma}$ matrices that we actually used, with components of $\mathbf{g}$ ranging from -10 to $+10$ in all directions, are of size 9260×9260 and thus clearly beyond the capability of standard inversion techniques. Such sizes are necessary in order to get accurate, reliable results at large contrasts between the two components.[22]

All of the results that are reported here are converged, as far as their dependence on the size of the matrix $\Gamma_{\mathbf{g}\mathbf{g}'}$ is concerned. However, the series (9) only converges when $\mathbf{H}$ is not very strong, i.e., when $\sigma_{xy} \leq \sigma_{xx}$, at least in the $\hat{\sigma}_2$ component. For larger values of $\mathbf{H}$, Padé approximants, as well as other standard methods, were used in order to sum the divergent series, based on a detailed understanding of its analytic properties.[21] This approach is similar to one that has been used recently for calculating the bulk effective dielectric properties of a periodic composite.[22] Here we only mention the fact that the reason why those methods are so effective in summing that series is that the operator $\hat{\Gamma}$ is bounded and continuous. Therefore, the singularities of the function that the series (9) represents, which are essentially just the eigenvalues of $\hat{\Gamma}$, are a bounded discrete set of simple poles, which can be shown to lie inside the rectangle $0 < \mathrm{Re}(s) < 1$, $|\mathrm{Im}(s)| < H + 1$ [H is defined precisely after (12) below] in the complex s plane.[21]

Although our calculational procedure naturally evaluates $\hat{\sigma}_e$ given $\hat{\sigma}_1$, $\hat{\sigma}_2$, and $\theta_{\mathbf{g}}$, the *physical* implications are best described and discussed by referring to the resistivity tensors $\hat{\rho}^{(e)} \equiv \hat{\sigma}_e^{-1}$ and $\hat{\rho}_i \equiv \hat{\sigma}_i^{-1}$, $i = 1, 2$.

The resistivity tensor $\hat{\rho}_i$ for a free-electron metal has the form

$$(\hat{\rho}_i)_{\alpha\beta} = \begin{pmatrix} \rho_i & R_i\mathcal{H}_z & -R_i\mathcal{H}_y \\ -R_i\mathcal{H}_z & \rho_i & R_i\mathcal{H}_x \\ R_i\mathcal{H}_y & -R_i\mathcal{H}_x & \rho_i \end{pmatrix}, \tag{11}$$

where the Ohmic resistivity ρ_i and the Hall coefficient R_i are independent of the magnetic field. As it appears here, the magnetic field $\vec{\mathcal{H}}$ is measured in conventional units. It is convenient to define a dimensionless form $\mathbf{H}$ for the magnetic field by

$$\rho_i \mathbf{H} = R_i \vec{\mathcal{H}}. \tag{12}$$

In these units $H \equiv |\mathbf{H}| = \omega_c \tau$, where the cyclotron frequency of a conduction electron with effective mass m_e is given, in SI units, by $\omega_c = e|\vec{\mathcal{H}}|/m_e$, and τ is the conductivity relaxation time.

Following the above definitions, the conductivity tensor $\hat{\sigma}_i = \hat{\rho}_i^{-1}$, $i = 1, 2$, separated into symmetric and antisymmetric parts: $\hat{\sigma} = \hat{\sigma}_s + \hat{\sigma}_a$, may be written in the form

$$(\hat{\sigma}_i)_{\alpha\beta} = \frac{1}{\rho_i(1+H^2)} \begin{pmatrix} 1+H_x^2 & H_xH_y & H_zH_x \\ H_xH_y & 1+H_y^2 & H_yH_z \\ H_zH_x & H_yH_z & 1+H_z^2 \end{pmatrix} + \frac{1}{\rho_i(1+H^2)} \begin{pmatrix} 0 & H_z & -H_y \\ -H_z & 0 & H_x \\ H_y & -H_x & 0 \end{pmatrix}. \quad (13)$$

We restrict ourselves to two types of materials: (a) composites with spherical inclusions and (b) composites with cylindrical inclusions. A picture of the different types of unit cells that were used in this study is shown in Fig. 1, while analytic expressions for the appropriate $\theta_{\mathbf{g}}$ functions are given in Table I. Other shapes of inclusions can be treated by using the expressions for $\theta_{\mathbf{g}}$ provided in Ref. 21.

We begin our analysis with a single inclusion, assuming it has spherical shape [see Fig. 2(a)], placed in a homogeneous conducting medium. The coordinate axes are just the cubic symmetry axes, and those will usually be used to characterize and evaluate the components of resistivity or conductivity tensors. At first we assume that the magnetic field is directed along the z axis. Then the longitudinal component $\rho_{\parallel}^{(e)}$ of the bulk effective resistivity tensor $\hat{\rho}^{(e)}$ is just $\rho_{zz}^{(e)}$. The two transverse components $\rho_{\perp}^{(e)} \equiv \rho_{xx}^{(e)}$ and $\tilde{\rho}_{\perp}^{(e)} \equiv \rho_{yy}^{(e)}$ are then equal. When we rotate $\mathbf{H}$ in the y, z plane, $\rho_{xx}^{(e)}$ remains one of the transverse components of $\hat{\rho}^{(e)}$, and we will continue to denote it by $\rho_{\perp}^{(e)}$. The other transverse component, denoted by $\tilde{\rho}_{\perp}^{(e)}$, as well as the longitudinal component of $\hat{\rho}^{(e)}$, will lie along two directions in the y, z plane which in general are not symmetry directions. Therefore, $\tilde{\rho}_{\perp}^{(e)}$ and $\rho_{\parallel}^{(e)}$ will then have to be calculated by applying to the tensorial components of $\hat{\rho}^{(e)}$ the appropriate rotation transformation $T(\xi)$ by an angle ξ in the y, z plane [see Fig. 2(b)]

$$\hat{\rho}_{\text{new}}^{(e)} = \hat{T}(\xi)\hat{\rho}^{(e)}\hat{T}^{-1}(\xi), \quad (14)$$

where

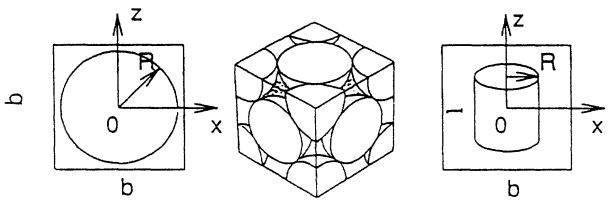

a. b. c.

FIG. 1. The different unit cells used in our calculations: (a) Single sphere (simple-cubic lattice). (b) fcc lattice of spheres. (c) Single cylinder (simple-cubic lattice). The size of the unit cell is $b \times b \times b$. The radii of the sphere and the cylinder are denoted by R, the length of the cylinder by l. The formulas for $\theta_{\mathbf{g}}$ corresponding to these unit cells are given in Table I.

$$\hat{T}(\xi) = \begin{pmatrix} \cos\xi & -\sin\xi & 0 \\ \sin\xi & \cos\xi & 0 \\ 0 & 0 & 1 \end{pmatrix}. \quad (15)$$

For other directions of $\mathbf{H}$, the transformation $\hat{T}$ must be generalized appropriately—in general, it will depend on three Euler angles which characterize the direction of $\mathbf{H}$ and that of the volume averaged current density $\langle \mathbf{J} \rangle$ in the fixed coordinate system.

III. SPHERICAL INCLUSIONS

Let us consider the case of a composite, made of identical spherical insulating inclusions which are placed periodically as a simple-cubic array inside a homogeneous conducting medium. As we explained above, we expect in this case different values for the three components $\rho_{\perp}^{(e)}, \rho_{\parallel}^{(e)}$, and $\tilde{\rho}_{\perp}^{(e)}$. In this section we will discuss in detail the angular profiles that were found for these components.

A. The transverse component along the (100) direction $\rho_{\perp}^{(e)}$

We first consider the case where the inclusions are perfectly insulating, i.e., $\hat{\sigma}_1 = 0$. In Fig. 3 we show results,

TABLE I. Fourier transforms of the characteristic functions corresponding to Fig. 1.

Figure	$\theta_{\mathbf{g}} = \frac{1}{V_b}\int_{V_b} \theta_1(\mathbf{r}) e^{-i\mathbf{g}\cdot\mathbf{r}} dV$
Sphere	$\theta_{\mathbf{g}} = [4\pi/(|g|b)^3]\,[\sin(|g|R) - |g|R\cos(|g|R)]$,
[see Fig. 1(a)]	where $|g| = \sqrt{g_x^2 + g_y^2 + g_z^2}$
fcc lattice of spheres	$\theta_{\mathbf{g}} = [\cos(g_x b/2) + \cos(g_y b/2) + \cos(g_z b/2)$
[see Fig. 1(b)]	$+\cos(g_x b/2) + \cos(g_y b/2)\cos(g_z b/2)]\theta_{\mathbf{g}}^{(\text{sphere})}$,
	where $\theta_{\mathbf{g}}^{(\text{sphere})} = \left[4\pi/(|g|b)^3\right]\,[\sin(|g|R) - |g|R\cos(|g|R)]$
Cylinder	$\theta_{\mathbf{g}} = \left(4\pi/g_{\perp}^3\right) RJ_1(Rg_{\perp})\,[\sin(|g_z|l/2)/|g_z|]$,
[see Fig. 1(c)]	where $J_1(x)$ is a Bessel function and $g_{\perp} = \sqrt{g_x^2 + g_y^2}$

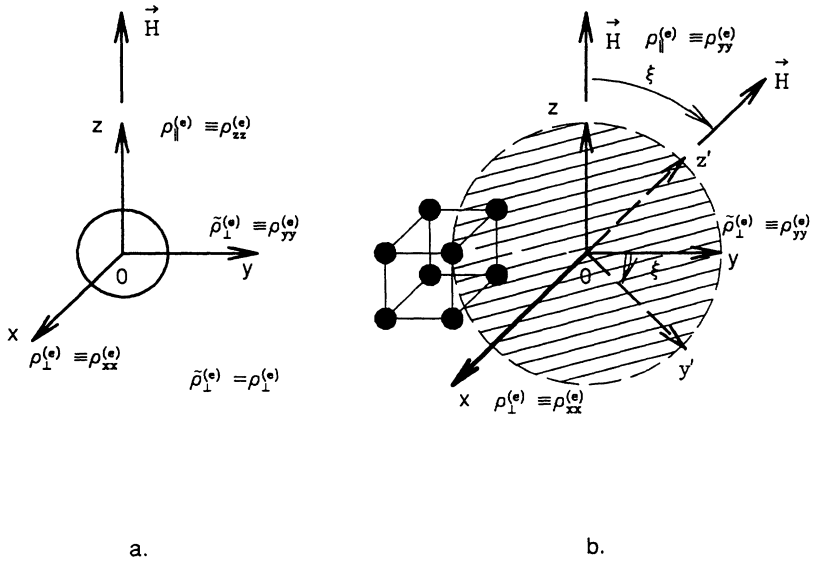

FIG. 2. (a) Schematic drawing of the coordinate system and direction of the magnetic field for a single sphere. The transverse magnetoresistances $\rho_{\perp}^{(e)} \equiv \rho_{xx}^{(e)}$ and $\tilde{\rho}_{\perp}^{(e)} \equiv \rho_{yy}^{(e)}$ have the same value. (b) The same for a composite with a simple-cubic array of spherical inclusions. The x axis is always directed along the lattice axis (100) and the magnetic field $\mathbf{H}$ is rotated in the y, z plane, making an angle ξ with the z axis. The first transverse component $\rho_{\perp}^{(e)} = \rho_{xx}^{(e)}$ represents the resistance when the average current $\mathbf{J}_0$ is directed along the lattice axis (100), while the other transverse component $\tilde{\rho}_{\perp}^{(e)}$ represents the resistance when $\mathbf{J}_0$ lies in the y, z plane, perpendicular to $\mathbf{H}$. For the special case where $\mathbf{H} \parallel z$, we can write $\rho_{\parallel}^{(e)} \equiv \rho_{zz}^{(e)}$ and $\tilde{\rho}_{\perp}^{(e)} \equiv \rho_{yy}^{(e)}$ (note that $\rho_{\perp}^{(e)} = \tilde{\rho}_{\perp}^{(e)}$ for a cubic lattice in this case).

obtained for the bulk effective transverse magnetoresistance $\rho_{\perp}^{(e)} \equiv \rho_{xx}^{(e)}$ in four samples with different sphere radii of the inclusions, when the magnetic field $\mathbf{H}$ has a fixed magnitude $|\mathbf{H}| \equiv H$ and is rotated in the y, z plane. The distance from the origin in these plots gives the magnitude of $\rho_{\perp}^{(e)}(\mathbf{H})/\rho^{(e)}(\mathbf{0}) - 1$ as a function of the direction of $\mathbf{H}$. Clearly, the magnetoresistance increases both with the sphere radius a and with H. For large enough H it develops a strong anisotropy, and the variations with the direction of $\mathbf{H}$ become more pronounced with increasing H and with decreasing a. The magnetoresistance eventually saturates with increasing H in any fixed direction, but this occurs more quickly at the minima. In fact, the deeper the minimum, the sooner the onset of saturation. The deepest minima are in the low order lattice directions equivalent to (001), then come those in the (011)-like directions, then (021), etc. For a given radius of the spheres only a finite number of minima appear, and the total number of minima increases with decreasing radius.

Although the number of minima observed in a given sample at first increases with H, the number saturates when H is large enough, even before the values of $\rho_{\perp}^{(e)}$ itself have saturated. To demonstrate this, we show in Figs. 4(a) and 4(b) a calculation of $\rho_{\perp}^{(e)}(\mathbf{H})$ for the same samples as in Figs. 3(a) and 3(b), but for larger values of H. The jagged features which appear in some places

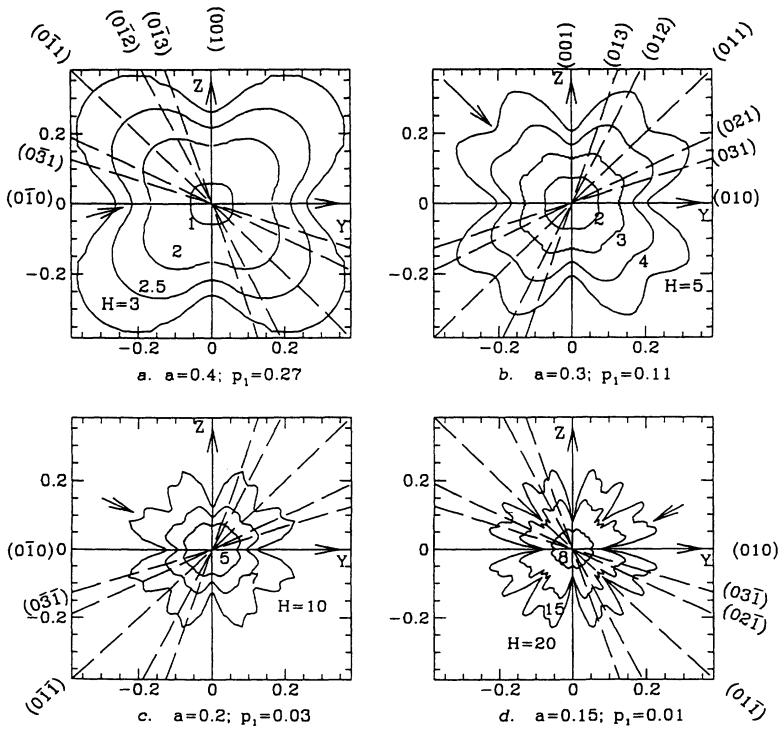

FIG. 3. Plots of the transverse magnetoresistance $\rho_{\perp}^{(e)} \equiv \rho_{xx}^{(e)}(\mathbf{H})$ for four samples of a cubic array of insulating spheres with radii $a = 0.40, 0.30, 0.20, 0.15$ and a lattice constant equal to 1, embedded in a free-electron host medium. The volume fraction of the spheres p_1 is shown in the figure. The relative transverse magnetoresistance $\delta\rho/\rho_0 \equiv \rho_{xx}^{(e)}(\mathbf{H})/\rho^{(e)}(\mathbf{0}) - 1$ is plotted for fixed $|\mathbf{H}| \equiv H$ as a function of the direction of $\mathbf{H}$ in the y, z plane. The magnitudes listed for H are actually the values of the dimensionless Hall to the Ohmic resistivity ratio ρ_{xy}/ρ_{xx} for the metallic host medium. The maximum number of minima in $\delta\rho/\rho_0$ increases by 1 along a new lattice axis each time the sphere radius is decreased along the sequence of values corresponding to the four samples of this figure. The new minimum which appears in each sample is highlighted by an arrow. The jagged oscillations which are evident in a few places in (a) and (b) are due to calculational errors and are discussed in the paper. The reciprocal lattice vectors used in these calculations ranged from -7 to 7 in each direction.

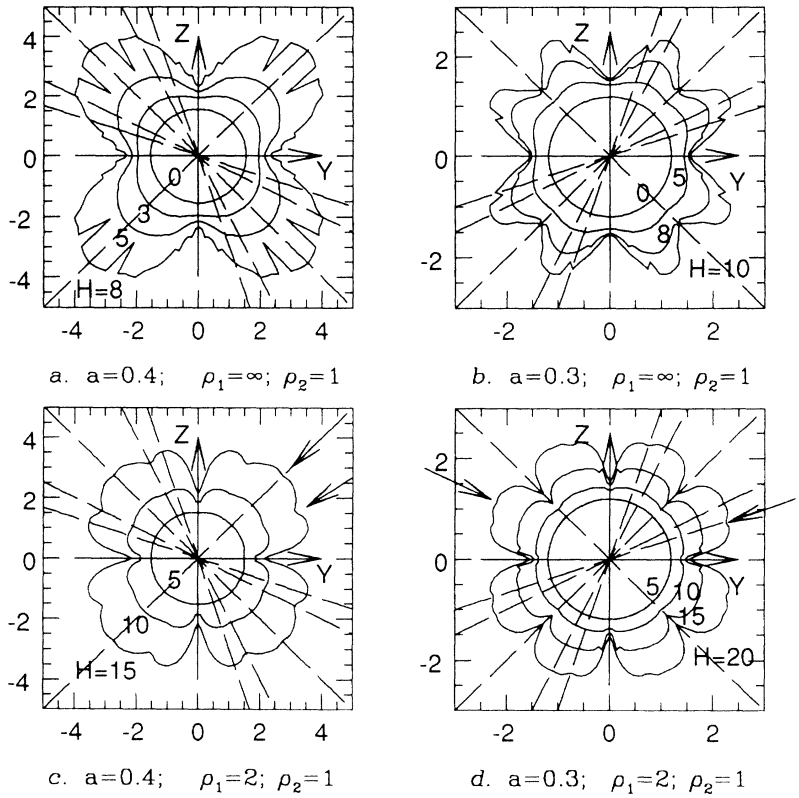

FIG. 4. (a) and (b) Plots of the absolute transverse magnetoresistance $\rho_{xx}^{(e)}(\mathbf{H})$ for the same two samples as in 3(a) and 3(b), but for larger values of H. Although the quality of the numerical results is poorer (the jagged oscillations are spurious, and are discussed in the paper), they show that the total number of minima has ceased to increase with H. All the results are for the case of perfectly insulating inclusions inside a conducting host: $\rho_1 = \infty$, $\rho_2 = 1$. (c) and (d) The same for the case when the inclusions have a finite resistivity which is different from that of the host material: $\rho_1 = 2$, $\rho_2 = 1$. The reciprocal lattice size used was the same as in Fig. 3.

in this figure, and also in a few places in Figs. 3(a) and 3(b), are due to imperfect convergence of the Padé approximants which we used in order to sum the divergent series. These spurious features can usually be differentiated from the true physical oscillations by the fact that they change their positions erratically when different elements of the Padé table are used or when H is changed. Their appearance is, therefore, indicative of the difficulties in our numerical procedure. The physical results for $\rho_{\perp}^{(e)}(\mathbf{H})$ are always smooth functions of $\mathbf{H}$.

All of these observations can be understood by considering the shape of the current distortion field $\mathbf{J}(\mathbf{r})$ which appears around a single insulating sphere of radius a in a uniform, free-electron metal when a current is made to flow that has a uniform value $\mathbf{J}_0$ far away from the obstacle. In the absence of a magnetic field, the distortion has a simple dipolar shape, so that the component of $\mathbf{J}-\mathbf{J}_0$ in the direction of $\mathbf{J}_0$ depends on the polar coordinates based on that direction according to $(3\cos^2\theta - 1)a^3/r^3$, where r is measured from the center of the obstacle. When a strong magnetic field $\mathbf{H} \perp \mathbf{J}_0$ is present, the distortion has a more complicated shape, but for an isolated insulating inclusion of either spherical or cylindrical shape, it has been solved exactly some years ago.[23] In Figs. 5–8 we reproduce some drawings of the current flow patterns and the local dissipation rates around such obstacles, taken from that reference. In the case of a spherical obstacle, $\mathbf{J}-\mathbf{J}_0$ has approximately the shape of a long cylinder of radius a and length $(\rho_{xy}/\rho_{xx})a$ in the direction of $\mathbf{H}$ [see Fig. 8(a)]. This produces an unsaturated magnetoresistance which increases approximately linearly with H.[23] When there is a finite density of spherical obstacles, these cylinders of distortion interact with one another and with other spheres, and this can lead to saturation of the magnetoresistance with increasing H. In a cubic array of spheres, this interaction will obviously be most effective when the cylinders of distortion lie along one of the (001) directions, and will be less effective if they lie along either a high index direction or a nonreciprocal-lattice direction. The value of H at which the interaction becomes effective and saturation begins to set in depends on the distance to the nearest sphere in the direction of the distortion cylinder axis, but also on the cylinder radius. If that radius is small enough, we can expect an oscillatory behavior of $\rho_{\perp}^{(e)}$ with changing direction for large enough values of H. The minima in this angular dependence will occur in the lowest index directions, i.e., (001), (011), etc. The maximum number of such minima, as well as their sharpness and depth, should increase with decreasing radius a. This number can be estimated from simple geometric considerations, in which we determine whether the cylinder of distortion, created by one supposedly isolated sphere and growing in length (but not in width) in a given direction with H, can reach its closest neighbor in that direction without first encountering other, closer spheres as a result of the finite radii [see Figs. 9(a) and 9(b)].

To see this, let us draw the normal from the center of the sphere B [see Fig. 9(b)] to a cylinder of distortion created by the sphere centered at point A. If the distance

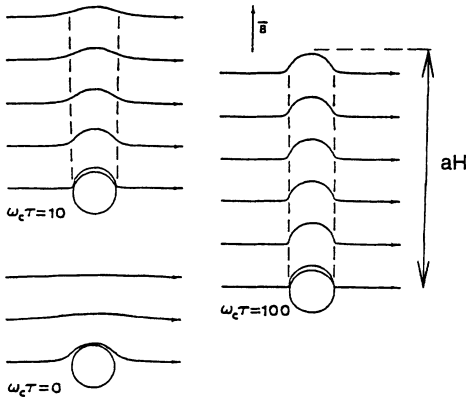

FIG. 5. Projection on the x, z plane of current lines (injected uniformly at $x = \infty$) in the region near a cylindrical void, for different values of $\omega_c\tau$. The dashed lines indicate regions of high current density (after Ref. 23). We have added to this figure an indication of the approximate total length of the distorted region, namely, $Ha = \omega_c\tau a$, where a is the cylinder radius.

BC is smaller than the sphere radius a, then the cylinder based upon the sphere A will be severely impeded by the sphere B before reaching D. But if BC is larger than a then the cylinder of distortion produced by A can extend unimpeded all the way to D, and we can expect that a minimum will appear in the magnetoresistance when **H** is in that direction. Using simple geometry we can write $BC = (BE - a) = (b\sin\theta - a)$, from which we get the condition $a \leq b\sin\theta/2$ for the appearance of that minimum, where θ is the angle between the (001) and the $(0n1)$ lattice axes $[\theta = \arcsin(1/\sqrt{1+n^2})]$ and b is the lattice constant of the cubic array. These considerations lead to the prediction that a minimum in the $(0n1)$ direction will appear at sufficiently large values of H whenever the sphere radius a satisfies the following inequality

$$\frac{a}{b} < \frac{1}{2\sqrt{1+n^2}}. \tag{16}$$

This criterion is in good *quantitative* agreement with our numerical results for $\rho_\perp^{(e)}$ (see Fig. 3).

The results, presented in Figs. 3, 4(a), and 4(b) were calculated for a composite with perfectly insulating inclusions (i.e., $\hat{\sigma}_1 = 0$). Results for some samples in which the inclusions have a nonzero conductivity that differs from that of the host material are shown in Figs. 4(c) and 4(d). In these samples, the conductivity tensor of the embedded inclusions was taken to be one-half of that of the host material. The similarity to the results for insulating inclusions is evident. A notable difference is the appearance (when $\hat{\sigma}_1$ is close to $\hat{\sigma}_2$) of additional minima [shown by the arrows in Figs. 4(c) and 4(d)]. In contrast to the case $\hat{\sigma}_1 = 0$, in the present case the single-spherical-inclusion problem is unsolved, and the method of Ref. 23 cannot be easily generalized to treat it. We, therefore, offer the following speculation: In the absence of a magnetic field,

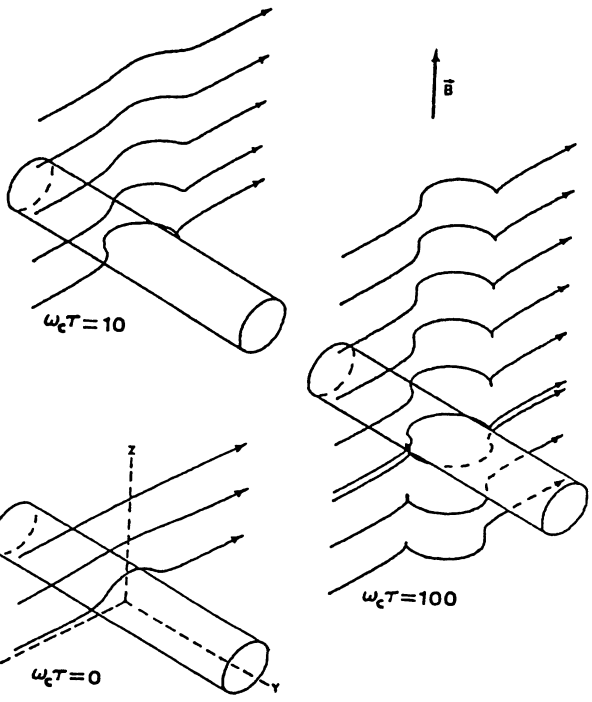

FIG. 6. Isometric projection of the current flow pattern of Fig. 5 illustrating the extent of S-shaped distortions and the high-density current sheets at large $\omega_c\tau$ (after Ref. 23). Note that the magnetic field **H** is denoted here by **B**.

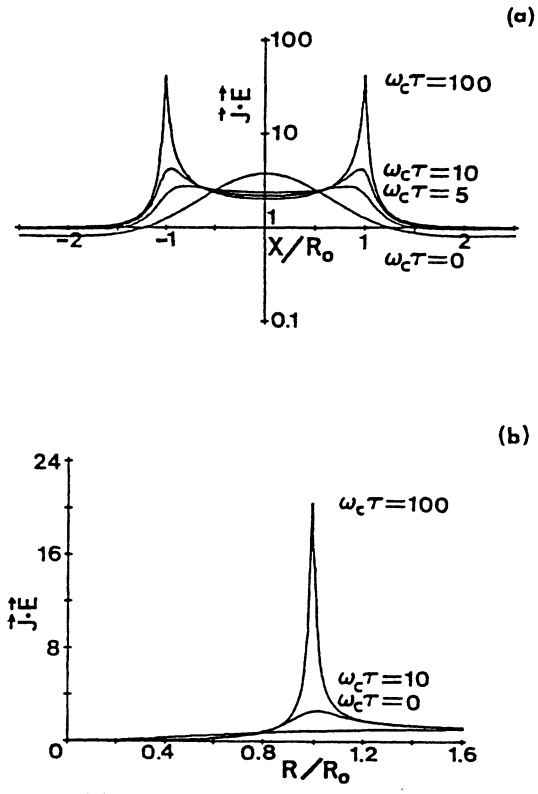

FIG. 7. (a) Volume power density $\mathbf{J} \cdot \mathbf{E}$ for the current distribution shown in Figs. 5 and 6 plotted along a line parallel to the x axis which touches the cylinder at $z = R_0$, the cylinder radius. (b) Radial dependence of the volume power density $\mathbf{J} \cdot \mathbf{E}$ for the current distribution shown in 8(b) plotted in the plane corresponding to $z = R_0$, the sphere radius (after Ref. 23).

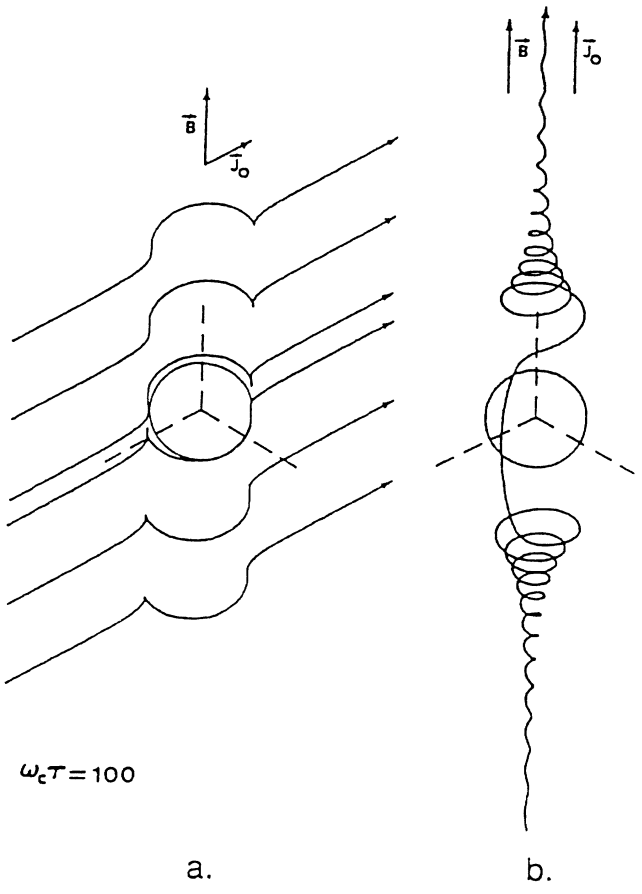

FIG. 8. (a) Isometric projection of current lines (injected uniformly at $x = \infty$) in the region near a spherical void when $\mathbf{J}_0 \perp B$. (b) Isometric projection of current lines (injected uniformly at $x = -\infty$) in the region near a spherical void when $\mathbf{J}_0 \parallel B$ (after Ref. 23). Note that the magnetic field $\mathbf{H}$ is denoted here by $\mathbf{B}$.

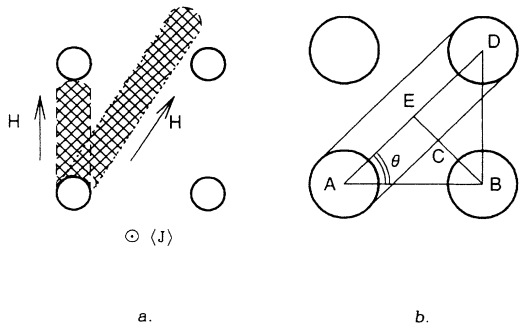

FIG. 9. (a) Schematic illustration showing how the onset of interference between the cylinders of current distortion from different spheres depends on the orientation of the magnetic field with respect to the lattice of obstacles. Note that the average current density $\langle \mathbf{J} \rangle$ is perpendicular to the plane of the page. (b) Schematic drawing used for the derivation of inequality (16) and showing the cylinder of current distortion with respect to the locations of the spherical inclusions.

the amplitude of current distortion around the obstacles is proportional to $a(1-\sigma_1/\sigma_2)$. If we assume that in the presence of a strong magnetic field H this is translated into a reduced effective radius $a_{\text{eff}} \equiv a(1-\sigma_1/\sigma_2)$ and reduced effective length $a_{\text{eff}}H$ of the cylinder of current distortion, then everything can be explained. Thus, for the case of conducting inclusions with $a = 0.4$ and $\hat{\sigma}_1 = \hat{\sigma}_2/2$ [see Fig. 4(c)] we get $a_{\text{eff}} = a/2 = 0.2$, which corresponds to the case of insulating inclusions shown in Fig. 3(c), with minima in the (011) and (021) directions. Note that, in the case of the insulating inclusions of radius 0.4, these two minima were not observed [see Fig. 3(a)]. Neither were they observed when we calculated the magnetoresistance for spheres of the same radius $a = 0.4$ and conductivity tensor $\hat{\sigma}_1 = \hat{\sigma}_2/10$. This is consistent with our hypothesis about the lengths, since, according to (16), when the effective radius is $a_{\text{eff}} = 0.4(1-0.1) = 0.36$, minima should appear only in the (001)-like directions and should not appear in other directions. The additional minima obtained when $\hat{\sigma}_1 \neq 0$ are very smooth and shallow, compared to the minima found also when $\hat{\sigma}_1 = 0$. We can, therefore, regard them as higher order minima and assume that the geometric mechanism of minima production described above and the inequality (16) apply to them as well.

B. The longitudinal component $\rho_{\parallel}^{(e)}$

The longitudinal component $\rho_{\parallel}^{(e)}$ for an arbitrary direction of $\mathbf{H}$ in the y,z plane was obtained using (14). For insulating inclusions, its angular dependence, shown in Fig. 10, is somewhat similar to that of $\rho_{\perp}^{(e)}$, but there are also some differences. For instance, $\rho_{\parallel}^{(e)}$ has a minimum in the (011) direction when $H = 8$ [see Fig. 10(c)]. This is in contrast with the behavior of $\rho_{\perp}^{(e)}$, which does not have a minimum there, in agreement with (16). This can be explained as follows: In the derivation of (16) we supposed that the volume of current distortions has a cylindrical shape. However, for the longitudinal case, where the average current is directed along $\mathbf{H}$, the distortion volume has approximately the shape of a skewed cone [see Fig. 8(b)]. Therefore, inequality (16) would need to be modified in order to describe the behavior of the longitudinal component.

C. The second transverse component $\tilde{\rho}_{\perp}^{(e)}$

In Fig. 10 we show, besides $\rho_{\perp}^{(e)}$ and $\rho_{\parallel}^{(e)}$, also $\tilde{\rho}_{\perp}^{(e)}$ as a function of the direction of $\mathbf{H}$ for different values of its magnitude. It is evident that this transverse magnetoresistance, which is not measured along a fixed lattice direction like $\rho_{\perp}^{(e)}$, exhibits behavior that is qualitatively different from that of $\rho_{\perp}^{(e)}$ for the same case of insulating spherical inclusions. In particular, $\tilde{\rho}_{\perp}^{(e)}$ has a sequence of maxima in the same directions where $\rho_{\perp}^{(e)}$ had minima. We were not able to find a simple geometric explanation

for this behavior, in contrast with the case of the minima in the angular dependence of $\rho_{\perp}^{(e)}$. However, we would like to offer some speculations about it.

In contrast with the case of $\rho_{\perp}^{(e)}$, when the direction of $\mathbf{H}$ changes in the y,z plane, so does the direction of flow of the average current density $\langle \mathbf{J} \rangle$, which is in the same plane but perpendicular to $\mathbf{H}$. Therefore, the geometric cross section presented by the obstacles to this flux is also changing. The geometric shadowing effects by collinear obstacles is greatest when $\langle \mathbf{J} \rangle$ lies along a low index direction of the lattice, and one might therefore naively expect the obstacles to be less effective in obstructing the flux in those directions, thus leading to a *lower* resistivity. This logic is clearly wrong when $\mathbf{H} = \mathbf{0}$, since then the resistivity is entirely isotropic. The above argument is fallacious because even a single obstacle of radius a does not simply cut a geometrically sharp hole of that radius in the flux, but causes it to deform in a more gradual, long range dipolar fashion. In fact, the short range current distortions are probably smaller when the average current is not along a low index lattice direction such as (001). When a strong magnetic field is turned on, we believe there are now two competing effects.

The first is that the current distortion is much sharper and, apart from extending as a long cylinder along $\mathbf{H}$, is actually much more localized in the close vicinity of the obstacle itself. That is why the naive picture of each obstacle cutting a geometrically sharp hole in the flux becomes more reasonable, and the geometrical shadowing effect would make the resistivity *smaller* in the lowest index directions. In fact, this is what we found to happen for both $\rho_{\perp}^{(e)}$ and $\rho_{\parallel}^{(e)}$.

But there is also another effect, namely, that for a general direction of $\langle \mathbf{J} \rangle$, the current distortions are less pronounced even when $\mathbf{H} = \mathbf{0}$. Therefore, the additional distortion that appears when $\mathbf{H} \neq 0$ is not as great as

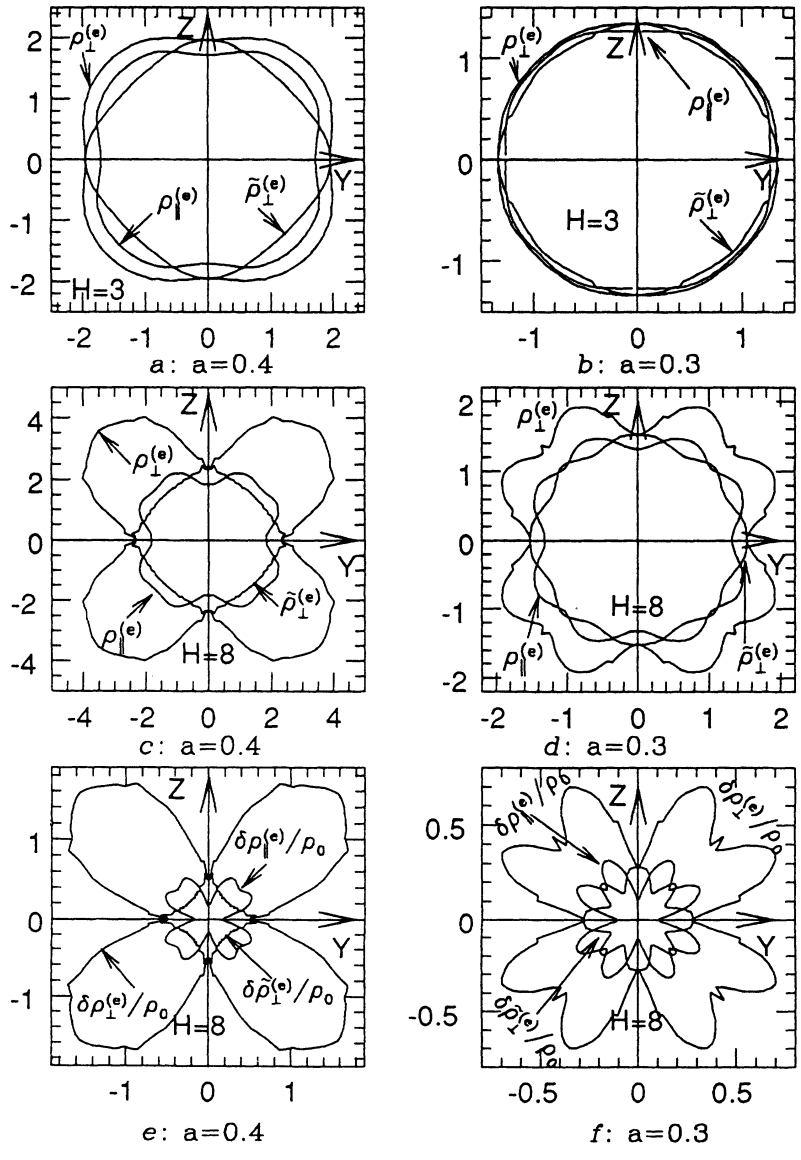

FIG. 10. Plots of the absolute (a)–(d) and relative [i.e., $\delta\hat{\rho}^{(e)}(\mathbf{H})/\rho^{(e)}(\mathbf{0}) \equiv \hat{\rho}^{(e)}(\mathbf{H})/\rho^{(e)}(\mathbf{0}) - 1$; $\rho^{(e)}(\mathbf{0})$ is denoted in the figure by ρ_0 for simplicity] (e) and (f) magnetoresistance components $\rho_{\perp}^{(e)}$, $\rho_{\parallel}^{(e)}$, and $\tilde{\rho}_{\perp}^{(e)}$ of two samples with a cubic array of insulating spheres with radii $a = 0.40$, 0.30 and a lattice constant equal to 1, embedded in a free-electron host medium. The reciprocal lattice size is the same as in Fig. 3.

in the (001) and other low index directions. This would lead us to expect a greater enhancement of the resistivity in the latter directions.

If the second effect is dominant, that could explain the maxima observed in $\tilde{\rho}_{\perp}^{(e)}$ in some of those directions. Clearly, this phenomenon needs to be studied further in order to determine whether these speculations are valid.

IV. CYLINDRICAL INCLUSIONS

In order to make quantitative predictions for possible experiments, the appropriate type of microstructure must be considered explicitly. Since it might be easier to produce a periodic composite where the inclusions have a cylindrical shape (e.g., by using lithographic techniques developed for microelectronics technology), we now consider a three-dimensional composite medium made of a three-dimensional simple-cubic array of parallel insulating cylinders of finite length embedded in a conducting host, with the cylinder axis along the (100) direction. Such a medium can be studied by the same methods that were used in Sec. III.

We now take **H** to be perpendicular to the cylindrical symmetry axis. In the strictly two-dimensional case of infinite cylinders, there is no magnetoresistance in composites made from materials which have no intrinsic magnetoresistance when **H** is parallel to the cylinder axes.[24] However, since the composite under consideration is in fact three dimensional, and since **H** is perpendicular to that axis, we do find magnetoresistance, and moreover, there appears a strong dependence on the direction of **H**.

In order to show how the behavior changes gradually with the cylinder length l, we present in Fig. 11 results for four samples with different values of l, namely $l = 0.6, 0.7, 0.95$, and 1.0 (the last of these corresponds to infinitely long cylinders). The explicit form of $\theta_{\mathbf{g}}$ for cylindrical inclusions is shown in Table I. From Fig. 11 we see that $\rho_{\perp}^{(e)} \equiv \rho_{xx}^{(e)}$ decreases with increasing l and in the limit $l \to 1$ this component of $\hat{\rho}^{(e)}$ becomes a smooth circle with a radius that is independent of H, i.e., there is no magnetoresistance. Although this may appear similar to the exact result for two-dimensional composites, which was mentioned above, it is actually quite different: The two-dimensional theorem, which is proved in Ref. 24, states that there is no magnetoresistance in the plane of the sample when **H** is perpendicular to it, whereas here **H** is in that plane.

The reason why $\delta\rho_{\perp}^{(e)} \equiv \rho_{\perp}^{(e)}(\mathbf{H}) - \rho_{\perp}^{(e)}(\mathbf{0}) = 0$ when the cylinders are infinitely long is that in this case the current flow, which is everywhere along the cylinder axes, is unaffected by **H**: This is the case where the geometrical shadowing effect is perfect. The other components of $\hat{\rho}^{(e)}$, namely $\rho_{\parallel}^{(e)}$ and $\tilde{\rho}_{\perp}^{(e)}$, do depend upon **H**. Their behavior is qualitatively similar to what was found in the case of spherical inclusions (in contrast with the behavior of $\rho_{\perp}^{(e)}$). In Fig. 12 we show all three magnetoresistance components $\rho_{\perp}^{(e)}$, $\rho_{\parallel}^{(e)}$, and $\tilde{\rho}_{\perp}^{(e)}$ for infinitely long cylin-

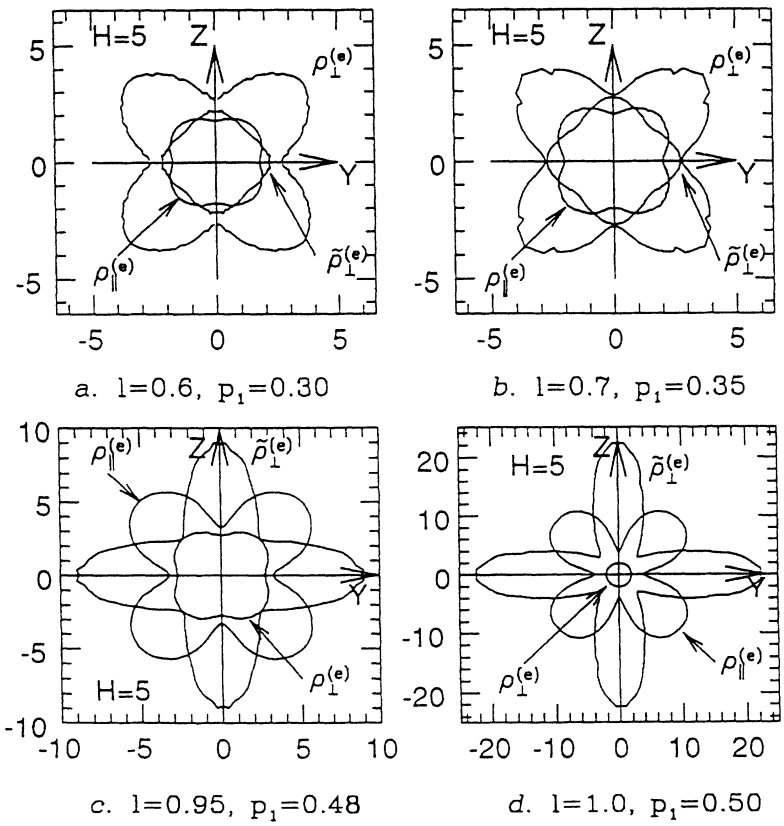

FIG. 11. Plots of the absolute magnetoresistance components $\rho_{\perp}^{(e)}$, $\rho_{\parallel}^{(e)}$, and $\tilde{\rho}_{\perp}^{(e)}$ of four samples of a cubic array of cylinders with the same radius $a = 0.4$, but different lengths l: l=0.6, 0.7, 0.95, and 1. The cylinders are perfect insulators and the host material is a free-electron metal. By increasing l, the value of $\rho_{\perp}^{(e)}$ decreases and its angular dependence becomes smoother, finally reducing to a circle of radius that is independent of H when $l = 1$. The behavior of $\rho_{\parallel}^{(e)}$ and $\tilde{\rho}_{\perp}^{(e)}$ is, in general, similar to the case of spherical inclusions; however the effect is much stronger. The jagged oscillations have the same spurious nature and origin as in Figs. 3 and 4, and are discussed in the paper. The resistivity $\tilde{\rho}_{\perp}^{(e)}$ becomes very large when $l \to 1$, which corresponds to infinitely long cylinders. The reciprocal lattice size is the same as in Fig. 3.

ders with radii $a = 0.40$, 0.30, and 0.20 at different values of H. The appearance of maxima and minima is in accordance with the scheme described in Sec. III for a cubic array of spheres.

In Fig. 13 we show results for $\tilde{\rho}_{\perp}^{(e)}$ in the (010) direction as a function of the magnetic field strength H. For cylinders of finite length, $\tilde{\rho}_{\perp}^{(e)}$ saturates with increasing H, as expected. But for $l = 1$, when the cylinders are infinitely long, there is no saturation. This can be understood as follows: From the exact solution for a single insulating cylindrical inclusion of infinite length, we know that even when the field $\mathbf{H}$ and the average current $\mathbf{J}_0$ are perpendicular to the cylinder axis, the distorted current has a component that is parallel to that axis[23] (see Fig. 6). Such a component will also be present in the case of an array of parallel cylinders, and it will increase with H without saturating, because of the perfect geometric shadowing effect along the cylinder axes. This will produce a correspondingly nonsaturating increase of $\tilde{\rho}_{\perp}^{(e)}$ with H.

One might speculate that the latter effect could be present, to some extent, also in the case of an array of spherical inclusions. If so, that would tend to produce a *maximum* rather than a *minimum* in the resistivity along a low index lattice axis, as was observed to occur in the case of $\tilde{\rho}_{\perp}^{(e)}$.

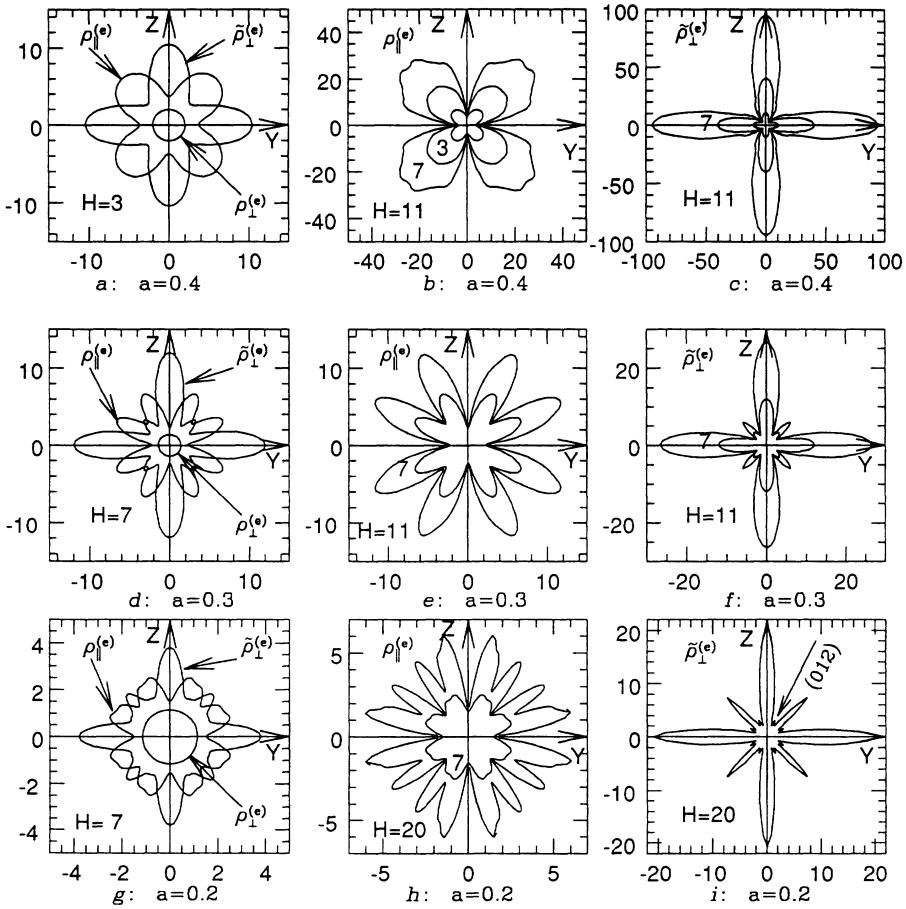

FIG. 12. Plots of the absolute magnetoresistances (the components $\rho_{\perp}^{(e)}$, $\rho_{\parallel}^{(e)}$, and $\tilde{\rho}_{\perp}^{(e)}$) of three samples with a two-dimensional square array of infinitely long cylinders with axes in the x direction and radii $a = 0.4$, 0.3, and 0.2. The component $\rho_{\perp}^{(e)}$ has no field dependence and is entirely isotropic [see the circle in the center of (a), (d), and (g)]. The other two components exhibit strong angular dependences. In the first column [(a), (d), and (g)] all three components are shown for a single value of H, while in the second column [(b), (e), and (h)] only $\rho_{\parallel}^{(e)}$ is shown, but for different values of H, and in the third column [(c), (f), and (i)] only $\tilde{\rho}_{\perp}^{(e)}$ is shown, again for different values of H. The number of minima (for $\rho_{\parallel}^{(e)}$) or maxima (for $\tilde{\rho}_{\perp}^{(e)}$) increases by one along a new lattice axis each time the cylinder radius is decreased [this is in agreement with the inequality (16), even though we have no reason to believe that it should apply here]. Note that the small maxima in the (012)-like directions in (i), one of which is marked by an arrow, are *real*. The reciprocal lattice vectors used in these calculations ranged from -10 to 10 in each direction.

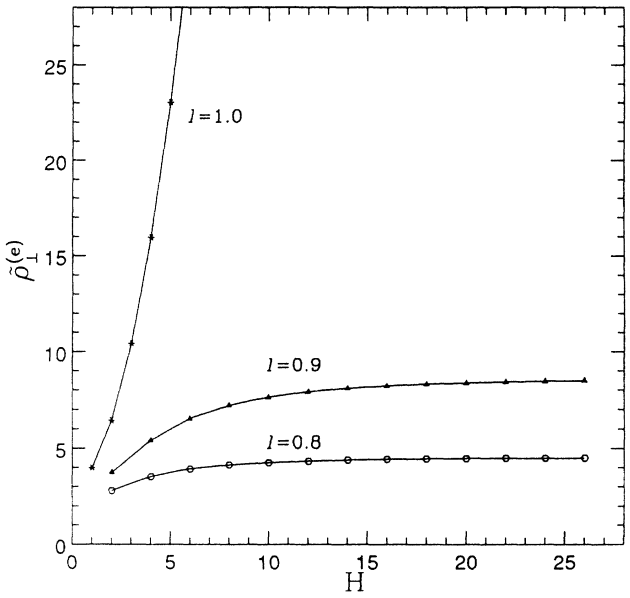

FIG. 13. (a) The y,z plane transverse effective resistance $\tilde{\rho}_\perp^{(e)}$ of three samples of cylinder arrays of lengths (in the x direction) $l = 0.8, 0.9, 1.0$ (the last case corresponds to infinitely long cylinders) as a function of the strength of the magnetic field H, which is always directed along the (010) axis. For cylinders of finite length, $\tilde{\rho}_\perp^{(e)}$ saturates as $H \to \infty$, but when that length is infinite, $\tilde{\rho}_\perp^{(e)}$ continues to increase without limit. The reciprocal lattice size was the same as in Fig. 12.

V. DISCUSSION AND SUMMARY

We have found that a new kind of anisotropic magnetoresistance should appear, at strong magnetic fields, in a periodic array of inclusions embedded in a conducting host, even when both components are free-electron metals, without any intrinsic magnetoresistance of their own. The anisotropy observed is a result of the strong Hall effect, but otherwise is a purely classical phenomenon. This means that in order to test our predictions an experiment should be done on a composite conducting medium in which the inclusions are large compared to the electron mean-free path and other microscopic lengths. From our physical understanding of the effect, it is clear that it must appear under quite general circumstances in a composite conductor with a periodic microstructure: The components need not be free-electron metals, they only need to have different magnetoconductivity tensors. These predictions clearly need to be tested experimentally.

Our intuitive physical understanding of the effects described in this paper is based on a geometrical picture of the interference between the current distortion fields produced by different inclusions. It is clearly incomplete because we have not been able to explain all the angular profiles that were found by the numerical calculations. More work needs to be done, perhaps including a detailed evaluation of the current distribution, in order to obtain a complete picture of what is happening and explain the numerically calculated angular profile of the magnetoresistance in all cases.

It is interesting to recall the fact that the full quantum-mechanical treatment of magneto-transport in a periodic crystal can also lead to a complicated and anisotropic magnetoresistance, due to a complex structure and connectivity of the Fermi surface. The fact that a periodic composite medium, which is a purely classical physical system, can give rise to such a similar behavior we find to be quite remarkable. We note that this similarity includes the fact that the minima in the angular dependence of $\rho_\perp$ for a crystal, when measured in a fixed lattice symmetry direction as a function of the direction of **H**, are also found to occur when **H** lies along the lowest index crystal axes [see, e.g., Refs. 20 and 25–27). The quantum case and the classical case have in common the periodic nature of the inhomogeneous microstructure, but they appear to have nothing else in common.

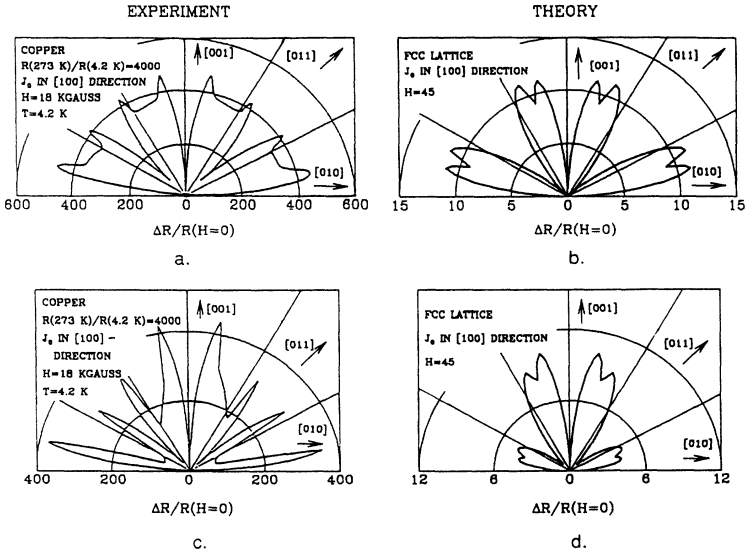

FIG. 14. Relative transverse magnetoresistance $\delta\rho/\rho_0$ in a fixed direction as a function of the magnetic field direction. In (a) and (b) the magnetic field is rotated in the plane perpendicular to the (100) axis, while in (c) and (d) it is rotated in the plane perpendicular to an axis inclined less than 3° away from the (100) axis. The results plotted on the left-hand side (a) and (c) are real experimental data obtained for copper at 18 000 G and 4.2 K in Ref. 25, while the plots on the right-hand side are our results, obtained by numerical computation for a fcc lattice of spherical inclusions. The striking difference between the two pairs of figures (a) and (b) and (c) and (d) is a result of the great sensitivity to sample orientation, as found both in the experiment (Ref. 25) and in our calculations.

We conjecture that this appearance is misleading, and that a quasiclassical treatment of the quantum problem may lead to the same kind of results that are traditionally found by considering the purely quantum-mechanical Fermi surface.[19] In support of these speculations we reproduce in Figs. 14(a) and 14(c) some experimental curves from Ref. 25, which describe the angular dependence of transverse magnetoresistance in a single crystal of very pure copper at liquid helium temperature, alongside results of some composite-medium-type calculations that we did on a face-centered-cubic (fcc) array of insulating spheres embedded in a free-electron host in Figs. 14(b) and 14(d) ($\theta_{\mathbf{g}}$ for this case is shown in Table I). The two sets of graphs cannot be compared quantitatively for a variety of reasons, among which is the fact that we do not know what value we should assign to our dimensionless parameter H. After this caveat, the similarity of shape between the two sets of graphs is nevertheless remarkable. This similarity may not seem entirely surprising if we recall the Drude theory of metals. The electron sea in that theory may be associated with the conducting host material, and the ionic core lattice with an array of insulating spherical inclusions, since the ionic core may be treated approximately as an insulator: all its bound electronic levels are filled, and the electrons from the sea of itinerant electrons cannot penetrate inside the ionic core. A more precise description (i.e., the electron shells are not exactly spherical and are not totally impenetrable) would introduce corrections. These ideas are currently being pursued in using a semiclassical approach to the quantum description of electronic motion in a potential in the presence of a magnetic field.

It may seem that our calculation sheds no light on real composite materials. It is true that most composite materials used in present day technology are not sufficiently ordered or periodic for our analysis to apply. However, truly periodic (though nonconducting) composites have recently been made in connection with the quest for a photonic band gap.[28,29] We now hope that material scientists will try to make periodic composites which are conducting, in order to try and observe some of the new behavior that we have predicted here.

Finally, we consider some practical issues related to experimental testing of our predictions. As we showed earlier, it is possible to observe the anisotropy effect only when the magnetic field is strong enough, i.e., when $\rho_{xy} > \rho_{xx}$, or equivalently $H = \omega_c\tau > 1$, in the host medium. Since $\omega_c = e\mathcal{H}/m_e$ in SI units (m_e is the electron effective mass in kg, $\mathcal{H}$ is the magnetic field strength in T, e is the electronic charge in C), and since the relaxation time τ may be expressed in terms of the electric-field mobility of the electron $\mu = e\tau/m_e$, we can also rewrite this requirement as $H = \mu\mathcal{H} > 1$ (see Ref. 20). The mobility μ can have values within a very broad range, i.e., 10^{-7}–10 $\mathrm{m^2/V\,sec}$, and depends on the materials used as well as on the temperature, since the electron-phonon interaction and the scattering by imperfections and impurities both affect the value of μ. It is possible to achieve the condition $H > 1$, even with a field as low as 1 T, by working at liquid helium temperatures and using extremely pure copper or semiconductor films (see Ref. 20).

ACKNOWLEDGMENTS

This research was supported in part by grants from the U.S.-Israel Binational Science Foundation, the Israel Academy of Sciences and Humanities, and the Center for Absorption in Science and the Science Ministry of the State of Israel.

[1] U. Dai, A. Palevski, and G. Deutscher, Phys. Rev. B **36**, 790 (1987).
[2] M. Rhode and H. Micklitz, Phys. Rev. B **36**, 7289 (1987).
[3] H. Stachowiak, Physica **45**, 481 (1970).
[4] D. Stroud, Phys. Rev. B **12**, 3368 (1975).
[5] D. Stroud and F.P. Pan, Phys. Rev. B **13**, 1434 (1976).
[6] I. Webman, J. Jortner, and M.H. Cohen, Phys. Rev. B **15**, 1936 (1977).
[7] B.I. Shklovskii, Zh. Eksp. Teor. Fiz. **72**, 288 (1977) [Sov. Phys. JETP **45**, 152 (1977)].
[8] J.P. Straley, J. Phys. C **13**, 4335 (1980); **13**, L773 (1980).
[9] D.J. Bergman, Y. Kantor, D. Stroud, and I. Webman, Phys. Rev. Lett. **50**, 1512 (1983).
[10] D.J. Bergman, in *Annals of the Israel Physical Society, Vol. 5*, edited by G. Deutscher, R. Zallen and J. Adler (Adam-Hilger, London, 1983), pp. 297–321.
[11] D.J. Bergman and D. Stroud, Phys. Rev. B **32**, 6097 (1985).
[12] B. Ya. Balagurov, Fiz. Tverd. Tela **28**, 3012 (1986) [Sov. Phys. Solid State **28**, 1694 (1986)].
[13] D.J. Bergman, Philos. Mag. B **56**, 983 (1987).
[14] A.S. Skal, J. Phys. C **20**, 245 (1987).
[15] J.P. Straley, Phys. Rev. B **38**, 11 639 (1988).
[16] D.J. Bergman, E. Duering, and M. Murat, J. Stat. Phys. **58**, 1 (1990), and references therein.
[17] A.K. Sarychev, D.J. Bergman, and Y.M. Strelniker, Europhys. Lett. **21**, 851 (1993).
[18] A.K. Sarychev, D.J. Bergman, and Y.M. Strelniker, Phys. Rev. B **48**, 3145 (1993).
[19] I.M. Lifshits, M. Ya. Azbel, and M.I. Kaganov, *Electron Theory of Metals* (Consultants Bureau, New York, 1973).
[20] O. Madelung, *Introduction to Solid-State Theory* (Springer-Verlag, New York, 1978).
[21] D.J. Bergman and Y.M. Strelniker (unpublished).
[22] D. J. Bergman and K. J. Dunn, Phys. Rev. B **45**, 13 262 (1992).
[23] J.B. Sampsell and J.C. Garland, Phys. Rev. B **13**, 583 (1976). A detailed calculation of the current distortion around an isolated insulating obstacle of either spherical or cylindrical shape is given in this reference, along with some detailed illustrations of the flow patterns.
[24] D. Stroud and D. J. Bergman, Phys. Rev. B **30**, 447 (1984).
[25] J.R. Klauder and J.E. Kunzler, in *The Fermi Surface*, edited by W.A. Harrison and M.B. Webb (Wiley, New York, 1960), p. 125.
[26] C. Kittel, *Quantum Theory of Solids* (Wiley, New York,

1963), p. 239.
[27] N. E. Alekseevskii and Yu. P. Gaidukov, Zh. Eksp. Teor. Fiz. **36**, 447 (1959) [Sov. Phys. JETP **36**, 311 (1959)].
[28] E. Yablonovich, T.J. Gmitter, and K.M. Leung, Phys. Rev. Lett. **67**, 2295 (1991).
[29] K.M. Ho, C.T. Chan, and C.M. Soukoulis, Phys. Rev. Lett. **65**, 3152 (1990).